A Mach-Number-Weighted Nonlinear Multiscale Viscosity Method for the Compressible Navier–Stokes Equations

Elaine Bernine(✉), Isaac P. Santos, and Lucia Catabriga

Federal University of Espírito Santo, Vitória, Brazil
elaine.bernine@edu.ufes.br, {isaac.santos,lucia.catabriga}@ufes.br

Abstract. In this work, the nonlinear multiscale viscosity finite element method (NMV-YZβ_ω) is proposed for the numerical solution of the compressible Navier–Stokes equations. The formulation is based on the decomposition of the problem into macro and microscales within the framework of Variational Multiscale Stabilized Methods (VMS). A nonlinear artificial viscosity operator is introduced at both discretization scales, constructed from the YZβ discontinuity-capturing parameter and incorporating a Mach-number-dependent weighting. The method is validated through classical benchmark problems, including spatial convergence analyses and evaluation of numerical accuracy. The results demonstrate robust convergence and optimal rates in the L^2 and H^1 Sobolev norms, with solutions comparable to those obtained using the NMV-YZβ and NMV-CAU methods. Computational performance is also evaluated under different flow regimes. The proposed method exhibits performance comparable to that of the NMV-YZβ formulation, which in turn outperforms standard stabilized variational methods such as SUPG+YZβ and CAU, as well as the multiscale stabilized variational method NMV-CAU.

Keywords: Finite element · Compressible Navier–Stokes equations · Variational Multiscale Stabilized (VMS) · Nonlinear Multiscale Viscosity

1 Introduction

The compressible Navier–Stokes equations constitute the fundamental mathematical model for fluid flows with density variations and arise in many engineering and scientific applications. Due to their nonlinear and coupled structure, analytical solutions are rarely available, making numerical methods essential for their solution. In this context, the Finite Element Method (FEM) has been widely employed to obtain approximate solutions, particularly when combined with stabilization strategies capable of handling convection-dominated regimes.

This work was partially funded by CAPES and FAPES.

© The Author(s), under exclusive license to Springer Nature Switzerland AG 2027
O. Gervasi et al. (Eds.): ICCSA 2026 Workshops, LNCS 16759, pp. 55–72, 2027.
https://doi.org/10.1007/978-3-032-30518-3_4

Standard Galerkin finite element formulations are generally inadequate for compressible flows because they may exhibit numerical instabilities, such as spurious oscillations, loss of stability at high Reynolds number regimes, and difficulties in capturing sharp gradients associated with boundary layers and shock waves.

To mitigate these challenges, several variational stabilization techniques have been developed over the last four decades. Among the most widely used approaches are the stabilized variational methods *Consistent Approximate Upwind* (CAU) [1] and *Streamline Upwind Petrov-Galerkin* (SUPG) method with the YZβ discontinuity-capturing operator (SUPG+YZβ) [17–19]. In addition, multiscale stabilized variational methods have been proposed, including NMVC/NMV-CAU [4,5] and NMV-YZβ [2,3,5].

The CAU method was originally developed by Galeão and Do Carmo [9] for the advection-diffusion equation and incorporates a nonlinear discontinuity-capturing operator that acts along the gradient direction of the approximate solution, improving stability in regions with strong gradients. Later, the formulation was extended to the compressible Euler and Navier–Stokes equations using entropy variables [1], and subsequently reformulated in conservative variables [8].

The SUPG+YZβ formulation for compressible flows was introduced in [17–19] to reduce oscillations in regions with large gradients. In this approach, an adaptive artificial viscosity operator dynamically adjusts the diffusion level increasing stabilization in regions with steep gradients while preserving accuracy in smooth regions.

An alternative framework for stabilized finite element formulations is the *Variational Multiscale Stabilized* (VMS) method proposed by Hughes [12]. In this approach, the solution is decomposed into resolved (macroscale) and unresolved (microscale) components, allowing the influence of the unresolved scales to be incorporated into the numerical formulation. Applications of the VMS approach to compressible flows can be found in [13].

Within this multiscale framework, the *Nonlinear Multiscale Viscosity* (NMV) methods introduce nonlinear artificial viscosity operators at both discretization scales. Formulations based on the YZβ discontinuity-capturing parameter were proposed in [2,3], and later applied to the compressible Navier–Stokes equations in [5]. Bernine et al. [4] proposed the NMV-CAU method, extending the NMV framework to compressible Navier-Stokes by defining artificial viscosity from the CAU discontinuity-capturing parameter.

Numerical studies reported in [2–5] indicate that NMV-YZβ and NMV-CAU produce results comparable to those obtained with SUPG+YZβ and CAU methods, respectively, while exhibiting improved computational performance in terms of GMRES iterations and CPU time for both Euler and compressible Navier-Stokes problems. Motivated by these results, this work proposes a new formulation, denoted NMV-YZβ_ω, belonging to the class of NMV methods. The method introduces a nonlinear artificial viscosity operator at both discretization scales, constructed from the YZβ discontinuity-capturing parameter and incorporating a Mach-number-dependent weighting.

The remainder of this paper is organized as follows. Section 2 presents the governing equations of the compressible Navier-Stokes system. Section 3 introduces the proposed stabilized multiscale formulations, namely NMV-YZβ and NMV-YZβ_ω. Section 4 describes the temporal discretization procedure. Section 5 presents numerical experiments for subsonic, sonic, and transonic flow regimes, analyzing spatial convergence, accuracy, and computational performance. Finally, Sect. 6 summarizes the main conclusions.

2 Mathematical Formulation

The governing compressible Navier–Stokes equations are formulated from the conservation laws of mass, linear momentum, and energy, given respectively by

$$\frac{\partial \rho}{\partial t} + \frac{\partial}{\partial x_i}\left(\rho u_i\right) = 0, \quad \text{in } \Omega \times (0, t_f], \tag{1}$$

$$\frac{\partial (\rho u_i)}{\partial t} + \frac{\partial}{\partial x_j}\left(\rho u_i u_j + p\,\delta_{ij} - \sigma_{ij}\right) = f_i, \quad \text{in } \Omega \times (0, t_f], \tag{2}$$

$$\frac{\partial E_t}{\partial t} + \frac{\partial}{\partial x_i}\left[(E_t + p)u_i - \sigma_{ij}u_j + q_i\right] = 0, \quad \text{in } \Omega \times (0, t_f], \tag{3}$$

where ρ, u_i, p, σ_{ij}, f_i, E_t, and q_i, with $i, j = 1, 2$, denote, respectively, the density, the components of the velocity vector, the pressure, the components of the viscous stress tensor, the components of the body force per unit volume, the total energy and the components of the heat flux vector.

The viscous stress tensor is defined as $\sigma_{ij} = \lambda \frac{\partial u_k}{\partial x_k}\delta_{ij} + \mu\left(\frac{\partial u_i}{\partial x_j} + \frac{\partial u_j}{\partial x_i}\right)$, with $i, j, k = 1, 2$, where $\mu = \mu_0 \left(\frac{T}{T_0}\right)^{3/2} \frac{(T_0+S)}{(T+S)}$ is the dynamic viscosity coefficient, with S being the Sutherland constant, T the temperature and μ_0 and T_0 denoting reference values, and $\lambda = -\frac{2\mu}{3}$ is the second viscosity coefficient, considering the ideal gas (Stokes hypothesis).

When the fluid is considered as a perfect gas, and following the definitions presented in [16], we have $E_t = \rho\left(e_{in} + \frac{1}{2}u_i u_i\right) = \rho E$, which denotes the total energy per unit volume. Here, E is the total specific energy, $e_{in} = c_v T$ is the specific internal energy, $p = \rho R T$ is the pressure, $k = \gamma R \mu/(\gamma - 1)Pr$ is the thermal conductivity, c_v is the specific heat at constant volume, c_p is the specific heat at constant pressure, $\gamma = c_p/c_v$ is the adiabatic exponent, $R = c_p - c_v$ is the specific gas constant and Pr is the Prandtl number.

The compressible Navier–Stokes equations (1), (2) and (3) can be rewritten in vector form with coordinates $(x_1, x_2) \in \Omega \subset \mathbb{R}^2$ and time variable $t \in (0, t_f]$ as follows:

$$\frac{\partial \boldsymbol{U}}{\partial t} + \frac{\partial \boldsymbol{F}_i}{\partial x_i} - \frac{\partial \boldsymbol{G}_i}{\partial x_i} = \boldsymbol{S}, \tag{4}$$

where $\boldsymbol{U} = [\rho, \rho u_i, \rho E]^T$ is the vector of conservative variables and $\boldsymbol{S} = [0, f_i, 0]^T$ represents the body force per unit volume, with $i = 1, 2$. The Euler flux vectors,

$\boldsymbol{F}_i$ (advective transport terms), and the viscous flux vectors, $\boldsymbol{G}_i$ (diffusive transport terms), for $i = 1, 2$, are defined as:

$$\boldsymbol{F}_i = \begin{bmatrix} \rho u_i \\ \rho u_i u_1 + p\delta_{i1} \\ \rho u_i u_2 + p\delta_{i2} \\ (\rho E + p)\, u_i \end{bmatrix} \quad \text{and} \quad \boldsymbol{G}_i = \begin{bmatrix} 0 \\ \sigma_{1i} \\ \sigma_{2i} \\ \sigma_{ik} u_k - q_i \end{bmatrix},$$

where δ_{ij} is the Kronecker delta and q_i denotes the components of the heat flux vector. Furthermore, Eq. (4) can be rewritten in the quasi-linear form as

$$\frac{\partial \boldsymbol{U}}{\partial t} + \boldsymbol{A}_i \frac{\partial \boldsymbol{U}}{\partial x_i} - \frac{\partial}{\partial x_i}\left(\boldsymbol{K}_{ij} \frac{\partial \boldsymbol{U}}{\partial x_j}\right) = \boldsymbol{S}, \quad \text{in } \Omega \times (0, t_f], \tag{5}$$

where $\boldsymbol{A}_i = \dfrac{\partial \boldsymbol{F}_i}{\partial \boldsymbol{U}}$ denotes the Jacobian matrices associated with the advective transport in the x_i-direction, and $\boldsymbol{K}_{ij}$ represents the diffusion matrices such that $\boldsymbol{K}_{ij} \dfrac{\partial \boldsymbol{U}}{\partial x_j} = \boldsymbol{G}_i$, for $i, j = 1, 2$.

Related to Eq. (5), we consider the following initial and Dirichlet boundary conditions: $B\boldsymbol{U} = \boldsymbol{Z}$, on $\Gamma \times (0, t_f]$ and $\boldsymbol{U}(x_i, 0) = \boldsymbol{U}_0(x_i)$, with $i = 1, 2$, where Γ is the boundary of Ω, B is the boundary operator, and $\boldsymbol{Z}$ and $\boldsymbol{U}_0$ are known vector-valued functions.

3 Nonlinear Multiscale Variational Formulations

To apply the finite element method, we consider a disjoint partition of the domain Ω, denoted by $\mathcal{T}^h = \{\Omega^e\}_{e=1}^{nel}$, into nel linear triangular elements. For simplicity, only prescribed (Dirichlet) boundary conditions are considered. Let $\mathcal{S}^h$ denote the space of admissible functions and $\mathcal{V}^h$ the space of test functions, defined as follows:

$$\mathcal{S}^h = \{\boldsymbol{U}^h \in \left[H^1(\Omega)\right]^4; \quad \boldsymbol{U}^h|\Omega^e \in \left[\mathbb{P}^1(\Omega^e)\right]^4, \quad \boldsymbol{U}^h = \boldsymbol{Z} \text{ on } \Gamma\},$$
$$\mathcal{V}^h = \{\boldsymbol{W}^h \in \left[H^1(\Omega)\right]^4; \quad \boldsymbol{W}^h|\Omega^e \in \left[\mathbb{P}^1(\Omega^e)\right]^4, \quad \boldsymbol{W}^h = \boldsymbol{0} \text{ on } \Gamma\},$$

where $H^1(\Omega)$ denotes the Hilbert space of square-integrable functions whose first-order derivatives are also square-integrable, and $\mathbb{P}^1(\Omega^e)$ represents the set of linear polynomials defined on Ω^e.

The class of methods known as *Nonlinear Multiscale Variational* (NMV) formulations is characterized by the introduction of an additional term aimed at controlling the artificial viscosity of the system. The enriched solution and test spaces are defined as $\mathcal{S}^E = \mathcal{S}^h \oplus \mathcal{S}^b$ and $\mathcal{V}^E = \mathcal{V}^h \oplus \mathcal{V}^b$, where $\mathcal{S}^h$ and $\mathcal{V}^h$ denote the standard finite element spaces and $\mathcal{S}^b$ and $\mathcal{V}^b$ represent the bubble-function spaces, defined as follows:

$$\mathcal{S}^b = \{\boldsymbol{U}^b \in [H^1(\Omega)]^4;\ \boldsymbol{U}^b|_{\Omega^e} \in [\text{span}(\phi^b)]^4,\ \forall \Omega^e \in \mathcal{T}^h\},$$
$$\mathcal{V}^b = \{\boldsymbol{W}^b \in [H^1(\Omega)]^4;\ \boldsymbol{W}^b|_{\Omega^e} \in [\text{span}(\phi^b)]^4,\ \forall \Omega^e \in \mathcal{T}^h\}.$$

The cubic bubble function ϕ^b is defined on each element Ω^e as $\phi^b = 27N_1^e N_2^e N_3^e$, where $N_j^e = N_j^e(x, y)$ are the local basis functions associated with the space $\mathbb{P}^1(\Omega^e)$.

The NMV formulation for the compressible Navier–Stokes equations consists of finding $\boldsymbol{U}^E = \boldsymbol{U}^h + \boldsymbol{U}^b \in \mathcal{S}^E$, with $\boldsymbol{U}^h \in \mathcal{S}^h$ and $\boldsymbol{U}^b \in \mathcal{S}^b$, such that

$$\int_\Omega \left[\boldsymbol{W}^E \cdot \left(\frac{\partial \boldsymbol{U}^E}{\partial t} + \boldsymbol{A}_i^h \frac{\partial \boldsymbol{U}^E}{\partial x_i} \right) + \frac{\partial \boldsymbol{W}^E}{\partial x_i} \cdot \left(\boldsymbol{K}_{ij}^h \frac{\partial \boldsymbol{U}^E}{\partial x_j} \right) \right] d\Omega + \\ + \sum_{e=1}^{nel} \int_{\Omega^e} \delta_\nu(\boldsymbol{U}^h) \left(\frac{\partial \boldsymbol{W}^E}{\partial x_i} \cdot \frac{\partial \boldsymbol{U}^E}{\partial x_i} \right) d\Omega^e = \int_\Omega \boldsymbol{W}^E \cdot \boldsymbol{S}^E d\Omega, \tag{6}$$

for all $\boldsymbol{W}^E \in \mathcal{V}^E$, where $\boldsymbol{W}^E = \boldsymbol{W}^h + \boldsymbol{W}^b$, with $\boldsymbol{W}^h \in \mathcal{V}^h$ and $\boldsymbol{W}^b \in \mathcal{V}^b$. The term $\delta_\nu(\boldsymbol{U}^h)$ denotes a nonlinear parameter depending on $\boldsymbol{U}^h$, which regulates the amount of artificial viscosity introduced into the system.

3.1 Nonlinear Multiscale Variational Method NMV-YZβ

The NMV-YZβ method was initially introduced in [2,3] for the compressible Euler equations. Subsequently, in [5], its application was extended to the compressible Navier–Stokes equations. The variational formulation of this method is defined by Eq. 6, in which the artificial viscosity parameter is defined by the YZβ discontinuity-capturing parameter, that is, $\delta_\nu = \delta_{yz\beta}$, given by

$$\delta_{yz\beta}(\boldsymbol{U}^h) = \left\| \boldsymbol{Y}^{-1} \boldsymbol{R}_e(\boldsymbol{U}^h) \right\| \left(\sum_{i=1}^{2} \left\| \boldsymbol{Y}^{-1} \frac{\partial \boldsymbol{U}^h}{\partial x_i} \right\|^2 \right)^{\frac{\beta}{2}-1} \left\| \boldsymbol{Y}^{-1} \boldsymbol{U}^h \right\|^{1-\beta} \left(\frac{h_{yz\beta}}{2} \right)^{\beta}, \tag{7}$$

where $\boldsymbol{Y}$ is a diagonal matrix whose components are defined as $Y_r = U_r|_{\text{ref}}$, with $r = 1, 2, 3, 4$. The quantities $U_r|_{\text{ref}}$ represent the reference values of the conservative variables, assumed in this work as the initial condition of the problem. Moreover, $h_{yz\beta} = 2 \left(\sum_{a=1}^{3} |\mathbf{j} \cdot \nabla N_a| \right)$ denotes the local characteristic length of each element. Here, N_a represents the finite element shape function associated with node a, and $\mathbf{j} = \frac{\nabla \rho}{\|\nabla \rho\|}$ is the unit vector in the direction of the density gradient.

When considering $\beta = 1$ in the parameter $\delta_{yz\beta}$ defined in Eq. (7), the discontinuity-capturing operator introduces artificial viscosity into the system of equations with greater emphasis on regions with smooth gradients. On the other hand, when $\beta = 2$, the artificial viscosity acts predominantly in regions with steep gradients. Thus, in order to balance these effects, the parameter $\delta_{yz\beta}$ is defined as $\delta_{yz\beta}(\boldsymbol{U}^h) = \frac{1}{2} \left(\delta_{yz\beta}|_{\beta=1} + \delta_{yz\beta}|_{\beta=2} \right)$.

3.2 Nonlinear Multiscale Variational Method NMV-YZβ_ω

After studying the YZβ discontinuity-capturing parameter and the nonlinear artificial viscosity parameter dependent on the global Mach number, defined

in [3] for the Euler equations, the NMV-YZβ_ω method is proposed in this work for the compressible Navier–Stokes equations. This method consists of adding a nonlinear artificial viscosity term dependent on the Mach number in both scales of the problem. The variational formulation of the method is given by Eq. (6), with the artificial viscosity parameter defined as $\delta_\nu = \delta_\omega$, given by

$$\delta_\omega(\boldsymbol{U}^h) = (1 - \omega(M))\, \delta_{yz\beta}|_{\beta=1} + \omega(M)\delta_{yz\beta}|_{\beta=2},$$

where

$$\omega(M) = \frac{1}{4}\left(1 + \frac{1}{1 + \exp(-40\,(M-2))} + \frac{1}{1 + \exp(-40\,(M-0.3))}\right). \tag{8}$$

The function $\omega(M)$ is introduced to weight the action of the artificial viscosity added to the system, establishing a combination between the YZβ discontinuity-capturing parameters defined in Eq. (7) for $\beta = 1$ and $\beta = 2$. Its formulation aims to modulate the intensity of the stabilization according to the flow regime in each element of the domain. For $M < 0.3$, the function intensifies the contribution associated with regions with smooth gradients. Conversely, for $M > 2$, it increases the contribution related to regions characterized by steeper gradients. In the intermediate interval $0.3 \leq M \leq 2$, the weighting function promotes a smooth transition between these two behaviors, as shown in Fig. 1.

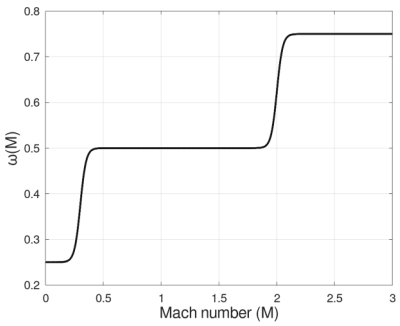


Fig. 1. Weighting function $\omega(M)$ defined in Eq. (8), considering $M \in [0, 3]$.

This weighting provides a smooth transition of the artificial viscosity across the different flow regimes. Consequently, the artificial viscosity parameter varies continuously with respect to M, ensuring a gradual transition between the different stabilization regimes and avoiding abrupt variations of the artificial viscosity parameter.

3.3 Local Matrices of the Variational Formulation

By applying the finite element approximations in the variational formulations of the NMV-YZβ_ω and NMV-YZβ methods, considering a triangular mesh and linear polynomial approximation, a local nonlinear system of differential-algebraic

equations is obtained, defined as follows:

$$\begin{bmatrix} \boldsymbol{M}^e_{hh} & \boldsymbol{M}^e_{hb} \\ \boldsymbol{M}^e_{bh} & \boldsymbol{M}^e_{bb} \end{bmatrix} \begin{bmatrix} \dot{\boldsymbol{\mathcal{U}}}_h \\ \dot{\boldsymbol{\mathcal{U}}}_b \end{bmatrix} + \begin{bmatrix} \boldsymbol{N}^e_{hh} & \boldsymbol{N}^e_{hb} \\ \boldsymbol{N}^e_{bh} & \boldsymbol{N}^e_{bb} \end{bmatrix} \begin{bmatrix} \boldsymbol{\mathcal{U}}_h \\ \boldsymbol{\mathcal{U}}_b \end{bmatrix} = \begin{bmatrix} \boldsymbol{S}_h \\ \boldsymbol{S}_b \end{bmatrix}, \tag{9}$$

where $\boldsymbol{\mathcal{U}}_h$ and $\boldsymbol{\mathcal{U}}_b$ are the vectors of nodal values associated with $\boldsymbol{U}^h$ and $\boldsymbol{U}^b$, respectively, for each element Ω^e, whereas $\dot{\boldsymbol{\mathcal{U}}}_h$ and $\dot{\boldsymbol{\mathcal{U}}}_b$ denote the corresponding vectors of time derivatives. The vectors $\boldsymbol{S}_h$ and $\boldsymbol{S}_b$ represent the nodal values of the source term components associated with the macro and microscales, respectively. The element mass matrices associated with Eq. (9) are defined as

$$\boldsymbol{M}^e_{pq} : \int_{\Omega^e} \boldsymbol{W}^p \cdot \frac{\partial \boldsymbol{U}^q}{\partial t}\, d\Omega^e, \qquad p, q \in \{h, b\},$$

and the element stiffness matrices are given by

$$\boldsymbol{N}^e_{pq} : \int_{\Omega^e} \left[\boldsymbol{W}^p \cdot \left(\boldsymbol{A}^h_i \frac{\partial \boldsymbol{U}^q}{\partial x_i} \right) + \frac{\partial \boldsymbol{W}^p}{\partial x_i} \cdot \left(\boldsymbol{K}^h_{ij} \frac{\partial \boldsymbol{U}^q}{\partial x_j} \right) + \delta_\nu(\boldsymbol{U}^h) \left(\frac{\partial \boldsymbol{W}^p}{\partial x_i} \cdot \frac{\partial \boldsymbol{U}^q}{\partial x_i} \right) \right] d\Omega^e,$$

with $p, q \in \{h, b\}$. Finally, the element load vectors are defined as

$$\boldsymbol{S}^e_p : \int_{\Omega^e} \boldsymbol{W}^p \cdot \boldsymbol{S}^p\, d\Omega^e, \qquad p \in \{h, b\}.$$

4 Time Integration Scheme

To advance the numerical solution in time for the compressible Navier–Stokes equations, given by Eq. (9), a time integration scheme is used based on the implicit predictor-multicorrector method described in [11]. This scheme adopts the formulation of the α-method, which establishes the relationships between the vectors of unknowns and their time discretized derivatives.

Using the relations of the generalized trapezoidal rule associated with the α-method, we obtain

$$\begin{aligned} \dot{\boldsymbol{U}}^{n+1,i+1}_p &= \dot{\boldsymbol{U}}^{n+1,i}_p + \Delta\dot{\boldsymbol{U}}^{n+1,i+1}_p, \\ \boldsymbol{U}^{n+1,i+1}_p &= \boldsymbol{U}^{n+1,i}_p + \alpha\Delta t \Delta\dot{\boldsymbol{U}}^{n+1,i+1}_p, \qquad p \in \{h, b\}. \end{aligned}$$

Thus, the system of Eqs. (9) can be rewritten in the form

$$\boldsymbol{M}_{hh}\dot{\boldsymbol{U}}^{n+1,i+1}_h + \boldsymbol{M}_{hb}\dot{\boldsymbol{U}}^{n+1,i+1}_b + \boldsymbol{N}_{hh}\boldsymbol{U}^{n+1,i+1}_h + \boldsymbol{N}_{hb}\boldsymbol{U}^{n+1,i+1}_b = \boldsymbol{S}^{n+1}_h, \tag{10}$$

$$\boldsymbol{M}_{bh}\dot{\boldsymbol{U}}^{n+1,i+1}_h + \boldsymbol{M}_{bb}\dot{\boldsymbol{U}}^{n+1,i+1}_b + \boldsymbol{N}_{bh}\boldsymbol{U}^{n+1,i+1}_h + \boldsymbol{N}_{bb}\boldsymbol{U}^{n+1,i+1}_b = \boldsymbol{S}^{n+1}_b. \tag{11}$$

Using the α-method relations in Eqs. (10) and (11), we obtain, respectively,

$$\boldsymbol{M}_1\Delta\dot{\boldsymbol{U}}^{n+1,i+1}_h + \boldsymbol{N}_1\Delta\dot{\boldsymbol{U}}^{n+1,i+1}_b = -\boldsymbol{R}_1, \tag{12}$$

$$\boldsymbol{M}_2\Delta\dot{\boldsymbol{U}}^{n+1,i+1}_h + \boldsymbol{N}_2\Delta\dot{\boldsymbol{U}}^{n+1,i+1}_b = -\boldsymbol{R}_2, \tag{13}$$

where

$$\boldsymbol{R}_1 = \left(\boldsymbol{M}_{hh}\dot{\boldsymbol{U}}_h^{n+1,i} + \boldsymbol{M}_{hb}\dot{\boldsymbol{U}}_b^{n+1,i}\right) + \left(\boldsymbol{N}_{hh}U_h^{n+1,i} + \boldsymbol{N}_{hb}U_b^{n+1,i}\right) - \boldsymbol{S}_h^{n+1},$$
$$\boldsymbol{R}_2 = \left(\boldsymbol{M}_{bh}\dot{\boldsymbol{U}}_h^{n+1,i} + \boldsymbol{M}_{bb}\dot{\boldsymbol{U}}_b^{n+1,i}\right) + \left(\boldsymbol{N}_{bh}U_h^{n+1,i} + \boldsymbol{N}_{bb}U_b^{n+1,i}\right) - \boldsymbol{S}_b^{n+1},$$
$$\boldsymbol{M}_1 = \boldsymbol{M}_{hh} + \alpha\Delta t\boldsymbol{N}_{hh}, \quad \boldsymbol{M}_2 = \boldsymbol{M}_{bh} + \alpha\Delta t\boldsymbol{N}_{bh},$$
$$\boldsymbol{N}_1 = \boldsymbol{M}_{hb} + \alpha\Delta t\boldsymbol{N}_{hb}, \quad \boldsymbol{N}_2 = \boldsymbol{M}_{bb} + \alpha\Delta t\boldsymbol{N}_{bb}.$$

Performing static condensation on Eqs. (13) yields

$$\Delta\dot{\boldsymbol{U}}_b^{n+1,i+1} = -\boldsymbol{N}_2^{-1}\left(\boldsymbol{R}_2 + \boldsymbol{M}_2\Delta\dot{\boldsymbol{U}}_h^{n+1,i+1}\right), \tag{14}$$

where $\boldsymbol{N}_2$ is an invertible 4×4 matrix at the element level. Substituting Eq. (14) into Eqs. (12) leads to the condensed system

$$\boldsymbol{M}^*\Delta\dot{\boldsymbol{U}}_h^{n+1,i+1} = \boldsymbol{F}^*,$$

where $\boldsymbol{M}^* = \left(\boldsymbol{M}_1 - \boldsymbol{N}_1\boldsymbol{N}_2^{-1}\boldsymbol{M}_2\right)$ and $\boldsymbol{F}^* = -\boldsymbol{R}_1 + \boldsymbol{N}_1\boldsymbol{N}_2^{-1}\boldsymbol{R}_2$.

Algorithm 1 describes the steps of the implicit predictor-multicorrector method applied to the system of equations obtained from the NMV formulations. In this context, Δt is the time step, α denotes the time integration parameter, the subscript n corresponds to the time step of the solution, i is the nonlinear iteration index, i_{MAX} is the maximum number of nonlinear iterations, t_f is the final time, and $\Delta\dot{\boldsymbol{U}}_h$ represents the increment of the time derivative during the nonlinear iteration. Since linear triangular elements are employed, the element matrices are computed explicitly, avoiding the need for numerical quadrature. In this work, $\alpha = 0.5$ is adopted in all experiments, leading to a second-order accurate time discretization for both the macro- and microscales.

5 Numerical Results

In this section, classical numerical experiments of fluid flows governed by the compressible Navier–Stokes equations are presented in order to analyze spatial convergence, evaluate the accuracy of the numerical approximation, and validate the implementation of the NMV-YZβ_ω method. To this end, the spatial convergence rate is investigated using the planar Couette problem, which admits a known analytical solution [14], considering the $L^2(\Omega)$ and $H^1(\Omega)$ Sobolev norms. In addition, numerical results are presented for the following benchmark problems: planar Couette flow, the Carter flat plate problem, and the flow over the NACA0012 airfoil, considering both transonic flow with $M_0 = 0.85$ and subsonic flow with $M_0 = 0.5$. The results obtained with the proposed NMV-YZβ_ω method are compared with those of the NMV-YZβ method in order to assess the effectiveness of the proposed approach.

In all experiments, the fluid is assumed to be a compressible gas with specific heat at constant volume $c_v = 717.5$ J/(kg·K), specific heat at constant pressure

Algorithm 1. NMV Predictor-Multicorrector Algorithm

Input: $\boldsymbol{U}_h^0$, $\dot{\boldsymbol{U}}_h^0$, $\boldsymbol{U}_b^0$ e $\dot{\boldsymbol{U}}_b^0$;
$t = 0$;
repeat ▷ Prediction phase
$t = t + \Delta t$;
$\boldsymbol{U}_h^{n+1,0} = \boldsymbol{U}_h^n + (1-\alpha)\,\Delta t\dot{\boldsymbol{U}}_h^n$; $\quad \dot{\boldsymbol{U}}_h^{n+1,0} = 0$;
$\boldsymbol{U}_b^{n+1,0} = \boldsymbol{U}_b^n + (1-\alpha)\,\Delta t\dot{\boldsymbol{U}}_b^n$; $\quad \dot{\boldsymbol{U}}_b^{n+1,0} = 0$;
$i = 0$;
repeat ▷ Multicorrection phase
▷ Residual calculation

$$\boldsymbol{R}_1^{n+1,i} = \left(\boldsymbol{M}_{hh}\dot{\boldsymbol{U}}_h^{n+1,i} + \boldsymbol{M}_{hb}\dot{\boldsymbol{U}}_b^{n+1,i}\right) + \left(\boldsymbol{N}_{hh}\boldsymbol{U}_h^{n+1,i} + \boldsymbol{N}_{hb}\boldsymbol{U}_b^{n+1,i}\right) - \boldsymbol{S}_h^{n+1};$$

$$\boldsymbol{R}_2^{n+1,i} = \left(\boldsymbol{M}_{bh}\dot{\boldsymbol{U}}_h^{n+1,i} + \boldsymbol{M}_{bb}\dot{\boldsymbol{U}}_b^{n+1,i}\right) + \left(\boldsymbol{N}_{bh}\boldsymbol{U}_h^{n+1,i} + \boldsymbol{N}_{bb}\boldsymbol{U}_b^{n+1,i}\right) - \boldsymbol{S}_b^{n+1};$$

$$\boldsymbol{M}_1 = \boldsymbol{M}_{hh} + \alpha\Delta t\boldsymbol{N}_{hh}; \qquad \boldsymbol{M}_2 = \boldsymbol{M}_{bh} + \alpha\Delta t\boldsymbol{N}_{bh};$$
$$\boldsymbol{N}_1 = \boldsymbol{M}_{hb} + \alpha\Delta t\boldsymbol{N}_{hb}; \qquad \boldsymbol{N}_2 = \boldsymbol{M}_{bb} + \alpha\Delta t\boldsymbol{N}_{bb};$$
$$M^* = \boldsymbol{M}_1 - \boldsymbol{N}_1\boldsymbol{N}_2^{-1}\boldsymbol{M}_2; \qquad F^* = -\boldsymbol{R}_1 + \boldsymbol{N}_1\boldsymbol{N}_2^{-1}\boldsymbol{R}_2;$$
$M^*\Delta\dot{\boldsymbol{U}}_h^{n+1,i+1} = F^*$; ▷ Preconditioned GMRES solver
▷ Correction phase

$$\boldsymbol{U}_h^{n+1,i+1} = \boldsymbol{U}_h^{n+1,i} + \alpha\Delta t\Delta\dot{\boldsymbol{U}}_h^{n+1,i+1};$$
$$\dot{\boldsymbol{U}}_h^{n+1,i+1} = \dot{\boldsymbol{U}}_h^{n+1,i} + \Delta\dot{\boldsymbol{U}}_h^{n+1,i+1};$$
$$\Delta\dot{\boldsymbol{U}}_b^{n+1,i+1} = -\boldsymbol{N}_2^{-1}\left(\boldsymbol{R}_2^{n+1,i} + \boldsymbol{M}_2\Delta\dot{\boldsymbol{U}}_h^{n+1,i+1}\right);$$
$$\boldsymbol{U}_b^{n+1,i+1} = \boldsymbol{U}_b^{n+1,i} + \alpha\Delta t\Delta\dot{\boldsymbol{U}}_b^{n+1,i+1};$$
$$\dot{\boldsymbol{U}}_b^{n+1,i+1} = \dot{\boldsymbol{U}}_b^{n+1,i} + \Delta\dot{\boldsymbol{U}}_b^{n+1,i+1};$$

$i = i + 1$;
until $i < i_{MAX}$
$n = n + 1$;
until $t < t_f$
Output: $\boldsymbol{U}_h^{t_f}$, $\dot{\boldsymbol{U}}_h^{t_f}$, $\boldsymbol{U}_b^{t_f}$ e $\dot{\boldsymbol{U}}_b^{t_f}$;

$c_p = 1004.5$ J/(kg · K), gas constant $R = 287$ J/(kg · K), adiabatic exponent $\gamma = 1.4$, and Prandtl number $Pr = 0.72$. The numerical simulations are performed using the GMRES solver with a maximum of 100 cycles, 30 vectors in the Krylov basis, a tolerance of 10^{-5}, three nonlinear corrections iterations (i_{MAX}), a BlockDiag preconditioner, and matrix-vector products computed using the element-by-element (EBE) storage structure, as considered in [8].

The reference values $U_i|_{\text{ref}}$, used in the construction of the YZβ discontinuity-capturing operator, are taken in all experiments as the values prescribed at the inlet boundary Γ_1, as indicated in the figures of the following sections.

The code was developed in the C programming language within the framework of a finite element library under continuous development at the Laboratory of Optimization and Computational Modeling of the Federal University of

Espírito Santo (LabOtiM/UFES[1]). Compilation and execution were performed using GCC (GNU Compiler Collection) version 11.4.0, with the -Ofast flag to maximize performance through aggressive optimizations, and the -Wall flag to enable all compiler warnings, thereby increasing the efficiency and robustness of the code. The numerical experiments were carried out on a machine equipped with an Intel® Core™ i5-1035G1 @ 1.00GHz processor, 8 GB of RAM, and Ubuntu 20.04.6 LTS operating system.

5.1 Spatial Convergence Analysis

To evaluate the spatial convergence rates, the two-dimensional planar Couette flow problem [14] is considered on the domain $\Omega = (0,1) \times (0,1)$. This configuration consists of a stationary lower plate and an upper plate moving with uniform velocity, as illustrated in Fig. 2. For this case, the fluid viscosity is defined as $\mu = 0.000018$ and the thermal conductivity as $\kappa = 0.0251125\ \mathrm{W\,m^{-1}\,K^{-1}}$.

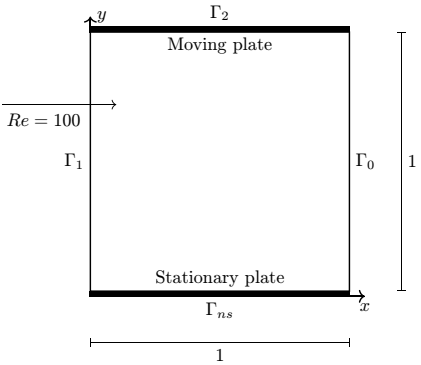


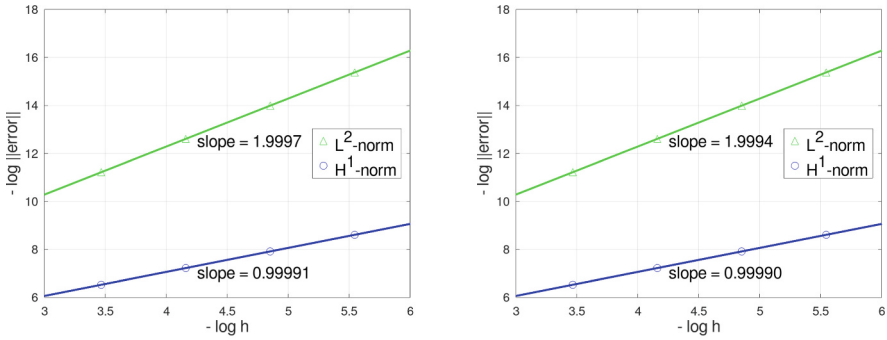
Fig. 2. Description of the planar Couette flow problem.

The boundary conditions are specified as follows: on Γ_1, the conservative variables are prescribed according to the exact solution of the problem, given by $\rho = T^{-1}$, $\rho u_1 = yT^{-1}$, $\rho u_2 = 0$, $\rho E = 2.5 + 0.5y^2T^{-1}$ and $T = 0.8 + 0.2y + \frac{\mu y^3}{2\kappa}(1-y)$; on Γ_2, the variables are prescribed as $\{U_1, U_2, U_3, U_4\} = \{1, 1, 0, 3\}$; on Γ_{ns}, all variables are prescribed as $\{U_1, U_2, U_3, U_4\} = \{1.25, 0, 0, 2.5\}$; and on Γ_0, a homogeneous Neumann (zero-flux) boundary condition is imposed.

Figures 3a and 3b present the spatial convergence rates of the density in the planar Couette problem, measured in the $L^2(\Omega)$ and $H^1(\Omega)$ norms using the NMV-YZβ_ω and NMV-YZβ methods, respectively. The simulations are performed on structured meshes with triangular elements of sizes $h \in$

[1] All experiment codes are available at https://github.com/mod-comp-ufes/FEM_CODES.

$\{2^{-5}, 2^{-6}, 2^{-7}, 2^{-8}\}$. The error norms between the exact and approximate solutions are evaluated at the final time $t_f = 10^{-3}$ seconds, considering a single time step of $\Delta t = 10^{-3}$, in order to eliminate the influence of the temporal error in the estimation of the spatial error. The results show that both the NMV-YZβ_ω and NMV-YZβ methods achieve optimal convergence rates close to 2 in the $L^2(\Omega)$ norm and 1 in the $H^1(\Omega)$ norm. These results confirm the expected asymptotic behavior of the methods and demonstrate their accuracy and numerical stability.



(a) NMV-YZβ_ω. (b) NMV-YZβ.

Fig. 3. Spatial convergence rates of the density error in the Couette problem measured in the L^2 and H^1 norms.

5.2 Carter Flat Plate Problem

The Carter flat plate problem is considered in over a two-dimensional domain $\Omega = (-0.2, 1.2) \times (0, 0.8)$ with Reynolds number $Re = 1000$ and Mach number $M_0 = 3$. The flat plate extends over the interval $0 \leq x \leq 1.2$, generating a boundary layer and a shock structure near the leading edge, as shown in Fig. 4. The thermal conductivity is taken as $\kappa = 1.395138\ \mathrm{W\,m^{-1}\,K^{-1}}$, and the temperature-dependent viscosity is modeled using Sutherland's law, $\mu = \dfrac{0.0906T^{1.5}}{T + 0.0001406}$, as described in [6,15].

The boundary conditions are prescribed as follows: on Γ_1, all variables are prescribed as $\{U_1, U_2, U_3, U_4\} = \{1, 1, 0, 0.698675\}$, with reference temperature $T_0 = 2.769 \times 10^{-4}$; on Γ_2, homogeneous Neumann boundary conditions are applied, with $U_3 = 0$; on Γ_{ns}, a no-slip condition is imposed, that is, $U_2 = U_3 = 0$, and a stagnation temperature $T_{\mathrm{stag}} = 7.7532 \times 10^{-4}$ is prescribed; and on Γ_0, a zero-flux boundary condition is imposed.

The numerical solutions were obtained at the final time $t_f = 3.5$ s using a structured mesh with 11421 nodes and 22400 triangular elements of size $h = 0.01$. Figures 5a and 5b show the density distributions obtained with the NMV-YZβ_ω and NMV-YZβ methods, respectively. The obtained results are consistent with

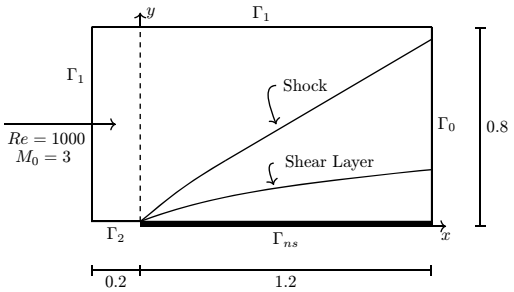
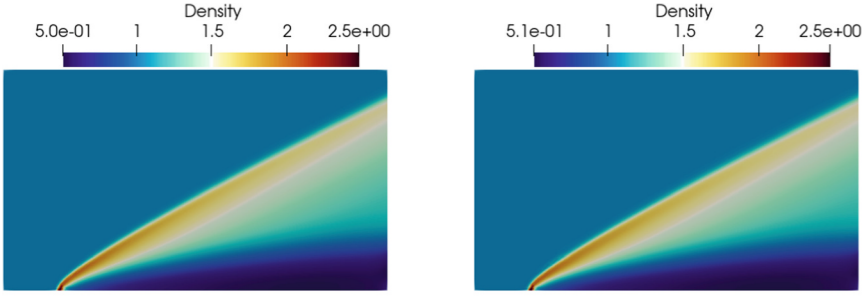


Fig. 4. Description of the Carter flat plate problem.

those reported in [1], which employed the CAU stabilization method, and in [4,5], where the nonlinear variational multiscale method NMV-CAU was used.



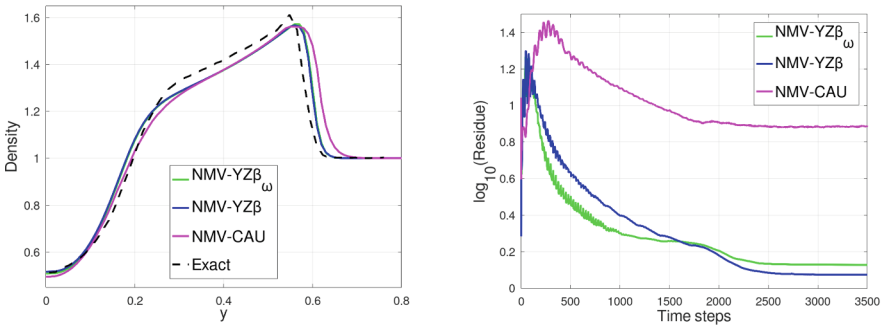
(a) NMV-YZβ_ω. (b) NMV-YZβ.

Fig. 5. Numerical results for density distributions in the Carter flat plate problem.

Figure 6a presents the density profiles for the Carter flat plate problem at $x = 1$, considering the NMV-YZβ_ω, NMV-YZβ, and NMV-CAU methods. The numerical results are compared with those reported in [7], obtained using the finite difference scheme of [10] and a mesh with triangular elements of size $h = 0.015$. The solutions obtained with the NMV-YZβ_ω and NMV-YZβ methods exhibit strong similarity, highlighting the consistency of the NMV-YZβ_ω multiscale formulation. Furthermore, these solutions are closer to the reference solution reported in [7] than the NMV-CAU solution.

Figure 6b shows the time evolution of the Euclidean norm of the density residuals for the Carter flat plate problem, considering the NMV-YZβ_ω, NMV-YZβ, and NMV-CAU methods. The NMV-YZβ_ω and NMV-YZβ methods present residuals with similar magnitude, with the NMV-YZβ_ω method achieving a greater reduction during the initial time steps. After approximately 1800 time steps, the NMV-YZβ method becomes more effective, producing smaller residu-

als. In contrast, the NMV-CAU method presents the largest residual magnitudes for this case.



(a) Density profile at $x = 1$. (b) Temporal variation of the residual.

Fig. 6. Numerical results for the Carter flat plate problem.

The computational performance results are presented in Table 1 for the Carter flat plate problem, using the NMV-YZβ_ω, NMV-YZβ, and NMV-CAU methods. The table summarizes the number of GMRES iterations and the CPU time spent for each method. The results show that the NMV-YZβ_ω method achieved the best computational performance, requiring 1198 fewer GMRES iterations than the NMV-YZβ method, while the NMV-CAU method presented the largest number of iterations among the methods analyzed. However, the CPU time is similar for all methods, being slightly lower for the NMV-YZβ_ω method.

Table 1. Computational performance of the Carter flat plate problem.

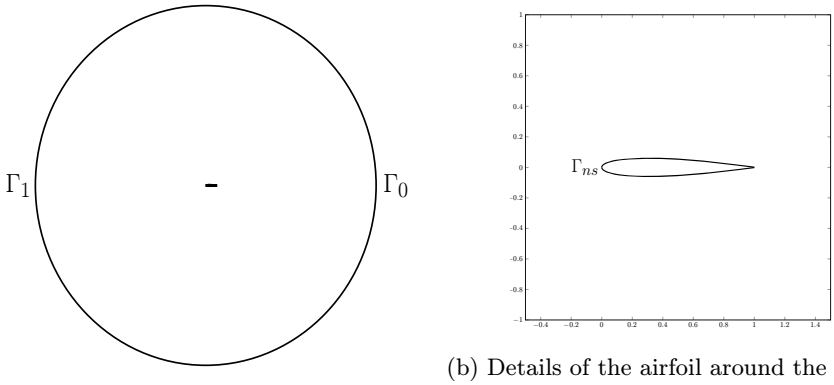
Methods	GMRES Iterations	CPU Time (s)
NMV-YZβ_ω	63051	1334.443
NMV-YZβ	64249	1346.938
NMV-CAU	67561	1368.057

5.3 Viscous NACA0012 Airfoil

The viscous NACA0012 airfoil problem is a two-dimensional case with a domain defined by a circle of radius 15, centered at the origin, in which the flow passes over the airfoil with an angle of attack of 0°, as illustrated in Fig. 7a. The aerodynamic profile considered in this study is defined by

$$y_t(x) = \pm 5t \left[0.2969\sqrt{x} - 0.1260x - 0.3516x^2 + 0.2843x^3 - 0.1015x^4\right], \quad (15)$$

where $x \in [0, 1]$ denotes the normalized position along the chord, and $t = 0.12$ represents the maximum thickness-to-chord ratio for the NACA0012 airfoil, as illustrated in Fig. 7b.



(a) General description.

(b) Details of the airfoil around the profile defined by Eq. (15).

Fig. 7. Description of the NACA0012 airfoil problem.

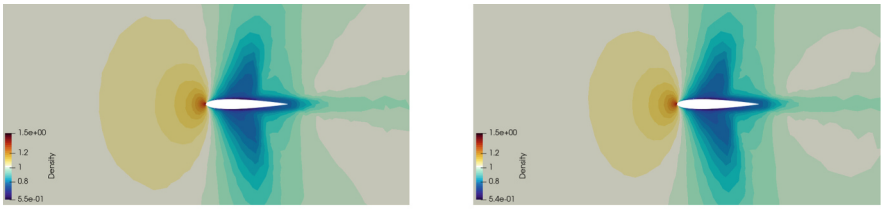
The boundary conditions are specified as follows: on Γ_1, corresponding to the region with $x \leq 0$ and $x^2 + y^2 = 15^2$, the variables $\{U_2, U_3, U_4\}$ are prescribed as $\{1, 0, c_v^* + 0.5\}$; on Γ_{ns}, defined by $y_t(x)$ in Eq. (15), no-slip conditions are imposed with $U_2 = U_3 = 0$ and stagnation temperature $T_{\text{stag}} = T_0 \left(1 + \frac{\gamma-1}{2} M_0^2\right)$; on Γ_0, corresponding to the region with $x > 0$ and $x^2 + y^2 = 15^2$, only the density is prescribed as $\rho = 1\ kg/m^3$. The dimensionless specific heat at constant volume depends on the inlet Mach number and is given by $c_v^* = \left(0.56 M_0^2\right)^{-1}$.

The numerical results for the viscous flow around the NACA0012 airfoil are presented for both the transonic regime with $M_0 = 0.85$ and the subsonic regime with $M_0 = 0.5$. The numerical solutions were obtained at the final time $t_f = 20$ seconds using an unstructured mesh composed of 2982 nodes and 5631 triangular elements.

Figures 8a and 8b present the numerical solutions for the viscous NACA0012 airfoil in the transonic regime with $M_0 = 0.85$, showing the density distributions obtained using the NMV-YZβ_ω and NMV-YZβ methods, respectively. The solutions obtained with both methods are similar. These numerical results align closely with those reported in [5,15].

Figure 10a shows the temporal evolution of the Euclidean norm of the density residuals for the viscous transonic NACA0012 airfoil problem with $M_0 = 0.85$, considering the NMV-YZβ_ω, NMV-YZβ, and NMV-CAU methods. The NMV-YZβ method presents the smallest residual magnitudes, whereas the NMV-CAU method produces the largest residuals. Overall, all three methods produce residuals of small magnitude.

The computational performance results for the NMV-YZβ_ω, NMV-YZβ, and NMV-CAU methods in the viscous transonic flow over the NACA0012 airfoil



(a) NMV-YZβ_ω. (b) NMV-YZβ.

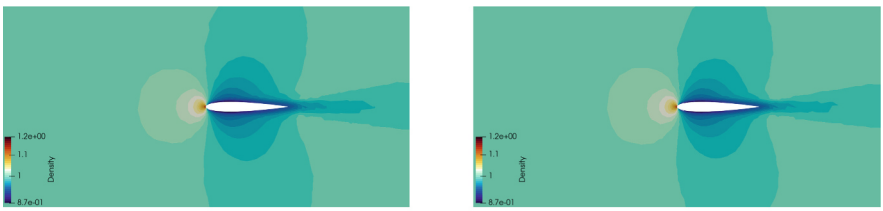
Fig. 8. Numerical results for the density distributions in the transonic NACA0012 airfoil problem with $M_0 = 0.85$.

are presented in Table 2. The results show that the NMV-YZβ method required 397 fewer GMRES iterations than the NMV-YZβ_ω method, while the NMV-CAU method presented the largest number of iterations among the analyzed methods. However, the CPU time for the NMV-YZβ_ω method is the lowest, being approximately 2.5% lower than that obtained with the NMV-CAU method, which presented the highest CPU time.

Table 2. Computational performance for the transonic NACA0012 airfoil problem.

Methods	GMRES Iterations	CPU Time (s)
NMV-YZβ_ω	359999	2023.721
NMV-YZβ	359602	2044.655
NMV-CAU	360378	2076.091

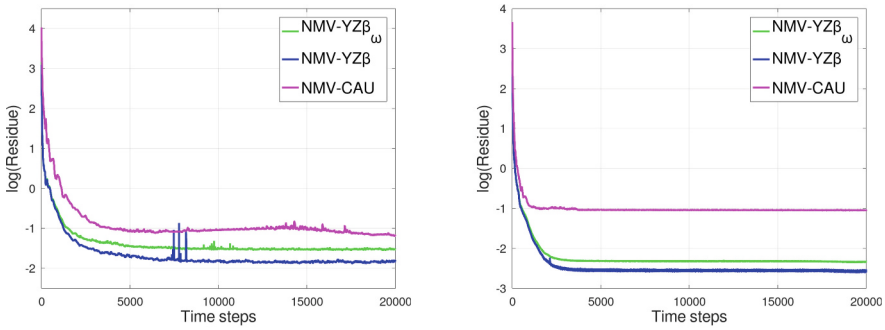
The Figs. 9a and 9b show the density distributions for the viscous NACA0012 airfoil in the subsonic regime with $M_0 = 0.5$, obtained with the NMV-YZβ_ω and NMV-YZβ methods, respectively. These solutions are similar and are also in good agreement with those reported in [5,15].



(a) NMV-YZβ_ω. (b) NMV-YZβ.

Fig. 9. Computed density distributions for the subsonic NACA0012 airfoil problem with $M_0 = 0.5$.

Figure 10b shows the temporal evolution of the Euclidean norm of the density residuals for the viscous subsonic NACA0012 airfoil problem using the NMV-YZβ_ω and NMV-YZβ methods. The NMV-YZβ method achieves the smallest residuals, although both methods reach similar orders of magnitude.



(a) Transonic - $M_0 = 0.85$. (b) Subsonic - $M_0 = 0.5$.

Fig. 10. Temporal evolution of the Euclidean norm of the density residual for the viscous NACA0012 airfoil problem.

The computational performance results for the viscous subsonic flow over the NACA0012 airfoil, using the NMV-YZβ_ω, NMV-YZβ, and NMV-CAU methods, are presented in Table 3. For this case, the NMV-YZβ_ω and NMV-YZβ methods required the same number of GMRES iterations. The Mach number takes values in the interval $[0, 0.58]$, including values $M < 0.3$, which led the NMV-YZβ_ω method to intensify the action of the parameter $\beta = 1$ in those regions. On the other hand, the NMV-CAU method presented the highest computational cost. However, the CPU times are similar among the analyzed methods, with the NMV-YZβ_ω method being approximately 1.5% faster than the NMV-CAU method.

Table 3. Computational performance for the subsonic NACA0012 airfoil problem.

Methods	GMRES Iterations	CPU Time (s)
NMV-YZβ_ω	359999	2025.696
NMV-YZβ	359999	2045.060
NMV-CAU	360455	2056.188

6 Conclusions

This work presented the multiscale variational method NMV-YZβ_ω for the solution of the compressible Navier–Stokes equations. This method decomposes

the problem of interest into two subproblems, corresponding to the macro and microscales, and introduces artificial viscosity at both discretization scales through the weighting of the YZβ discontinuity-capturing parameter.

The NMV-YZβ_ω, NMV-YZβ and NMV-CAU methods were applied to several benchmark problems governed by the compressible Navier–Stokes equations. The spatial convergence of the methods was investigated using the planar Couette problem, evaluating their behavior in the $L^2(\Omega)$ and $H^1(\Omega)$ norms. The accuracy of the formulations was further assessed through the Carter flat plate problem by comparing their numerical solutions with the reference solutions. In addition, numerical results were obtained for the NACA0012 airfoil problem under different flow regimes. The obtained solutions are consistent with those reported in the literature, confirming the validity of the proposed NMV-YZβ_ω method and its implementation.

Computational performance was also analyzed by comparing the NMV-YZβ_ω, NMV-YZβ, and NMV-CAU methods in terms of GMRES iterations and CPU time. The results indicate that the NMV-YZβ_ω method provides solutions comparable to those of the NMV-YZβ method while maintaining similar computational efficiency. Moreover, both approaches demonstrate superior performance with respect to the NMV-CAU method in terms of solution quality and computational cost.

Future work will focus on extending the proposed formulation to more challenging flow configurations, including three-dimensional problems and higher Reynolds number regimes. In addition, further investigations will consider the application of the NMV-YZβ_ω method to other compressible flow problems and the development of more efficient iterative solution strategies for large-scale simulations.

Acknowledgment. This study was financed in part by the Coordenação de Aperfeiçoamento de Pessoal de Nível Superior - Brasil (CAPES) - Finance Code 001 - and by the Fundação de Amparo à Pesquisa e Inovação do Espírito Santo (FAPES), Grant Notice No. 02/2026.

Declaration of Generative AI and AI-assisted technologies in the writing process. During the preparation of this work the authors used ChatGPT/OpenAI in order to improve language and readability. After using this tool, the authors reviewed and edited the content as needed and take full responsibility for the content of the published article.

References

1. Almeida, R.C., Galeão, A.C.: An adaptive Petrov–Galerkin formulation for the compressible Euler and Navier–Stokes equations. Comput. Methods Appl. Mech. Eng. **129**(1–2), 157–176 (1996)
2. Bento, S.S., de Lima, L.M., Sedano, R.Z., Catabriga, L., Santos, I.P.: A nonlinear multiscale viscosity method to solve compressible flow problems. In: Gervasi, O., Murgante, B., Misra, S., Rocha, A.M.A.C., Torre, C., Taniar, D., Apduhan, B.O.,

Stankova, E., Wang, S. (eds.) ICCSA 2016. LNCS, vol. 9786, pp. 3–17. Springer, Cham (2016). https://doi.org/10.1007/978-3-319-42085-1_1
3. Bento, S.S., Barbosa, P.W., Santos, I.P., de Lima, L.M., Catabriga, L.: A nonlinear finite element formulation based on multiscale approach to solve compressible Euler equations. In: Gervasi, O., et al. (eds.) ICCSA 2017. LNCS, vol. 10409, pp. 735–743. Springer, Cham (2017). https://doi.org/10.1007/978-3-319-62407-5_55
4. Bernine, E., Santos, I.P., Catabriga, L.: A nonlinear variational multiscale stabilized method for compressible Navier-Stokes equations. In: Gervasi, O., et al. (eds.) Computational Science and Its Applications – ICCSA 2024 Workshops. LNCS, vol. 14650, pp. 251–267. Springer, Cham (2024)
5. Bernine, E., Bento, S. S., de Lima, L. M., Santos, I. P., Catabriga, L.: Nonlinear stabilized multiscale methodologies for compressible Navier–Stokes equations. SSRN Electron. J. (2025)
6. Bonilla de Toro, J.: Implementation of finite element solvers for the compressible Navier–Stokes equations. PhD thesis, Universitat Politècnica de Catalunya (2015)
7. Carter, J.E.: Numerical solutions of the Navier-Stokes equations for the supersonic laminar flow over a two-dimensional compression corner. NASA Technical Report R-385 (1972)
8. Catabriga, L., Coutinho, A.L.G.A.: Implicit SUPG solution of Euler equations using edge-based data structures. Comput. Methods Appl. Mech. Eng. **191**(32), 3477–3490 (2002)
9. Galeão, A. C., do Carmo, E. G. D.: A consistent approximate upwind Petrov–Galerkin method for convection-dominated problems. Comput. Methods Appl. Mech. Eng. **68**(1), 83–95 (1988)
10. Godunov, S.K., Semendyaev, K.A.: Difference methods for the numerical solution of problems in gas dynamics. Zhurnal Vychislitel'noi Matematiki i Matematicheskoi Fiziki **2**(1), 3–14 (1962)
11. Hughes, T.J.R., Tezduyar, T.E.: Finite element methods for first-order hyperbolic systems with particular emphasis on the compressible Euler equations. Comput. Methods Appl. Mech. Eng. **45**(1–3), 217–284 (1984)
12. Hughes, T.J.R.: Multiscale phenomena: green's functions, the Dirichlet-to-Neumann formulation, subgrid scale models, bubbles and the origins of stabilized methods. Comput. Methods Appl. Mech. Eng. **127**(1–4), 387–401 (1995)
13. Koobus, B., Farhat, C.: A variational multiscale method for the large eddy simulation of compressible turbulent flows on unstructured meshes-application to vortex shedding. Comput. Methods Appl. Mech. Eng. **193**(15–16), 1367–1383 (2004)
14. Couette, M.: Études sur le frottement des liquides. Annales de Chimie et de Physique **21**, 433–510 (1890)
15. Parada, S., Codina, R., Baiges, J.: A VMS-based fractional step technique for the compressible Navier-Stokes equations using conservative variables. J. Comput. Phys. **459**, 111137 (2022)
16. Quarteroni, A.: Numerical Models for Differential Problems. Springer, Milan (2009)
17. Tezduyar, T.E.: Determination of the stabilization and shock-capturing parameters in SUPG formulation of compressible flows. In: Proceedings of the European Congress on Computational Methods in Applied Sciences and Engineering, ECCOMAS (2004)
18. Tezduyar, T.E., Senga, M.: Stabilization and shock-capturing parameters in SUPG formulation of compressible flows. Comput. Methods Appl. Mech. Eng. **195**(13–16), 1621–1632 (2006)
19. Tezduyar, T.E., Senga, M.: SUPG finite element computation of inviscid supersonic flows with YZβ shock-capturing. Comput. Fluids **36**(1), 147–159 (2007)